Transmittance and Bragg reflectivity of two-dimensional photonic lattices

Kazuaki Sakoda
Research Institute for Electronic Science, Hokkaido University, Kita-ku, Sapporo 060, Japan
(Received 20 March 1995; revised manuscript received 24 April 1995)

A general method based on the plane-wave expansion for calculating the transmittance and the Bragg reflectivity of two-dimensional photonic lattices is presented. According to this method, the transmission and the Bragg reflection spectra of a triangular and a square lattice of circular rods were numerically calculated for two independent polarizations. In addition to the opaque frequency ranges accompanied by the photonic band gaps, the existence of an uncoupled mode which cannot be excited by an external plane wave, a large amount of energy transfer to the Bragg waves, and pronounced interference structures were found. These three properties are not accounted for by the band calculation and the theoretical investigation which fully allows for the boundary condition at the surface of a specimen is necessary for proper understanding of experimental observations.

I. INTRODUCTION

Periodic dielectric structures, which are called photonic crystals or photonic lattices, have attracted much interest in recent years.[1–16] One of the reasons for the intense investigations, both theoretical and experimental, lies in the possibility of the substantial control of the radiation field by means of those structures. As was shown by Yablonovitch, Gmitter, and Leung,[3] a photonic band gap, or a frequency range in which the existence of any electromagnetic modes is forbidden, appears if the geometrical structure and the dielectric constant of the photonic lattice are appropriately chosen. Many peculiar physical phenomena due to the photonic band gap have been theoretically predicted: the suppression of spontaneous emission[1] and energy transfer,[5] the bound state of photons,[6] localized donor and acceptor modes,[2,10] etc. Among these predictions, the localized modes were observed for specimens that have a disorder in their regular lattices.[2,10] To my knowledge, experimental confirmation of the other phenomena has not been done yet.

The experimental investigation of the band structure of photonic lattices has mainly been carried out by observing the transmission spectra of the specimens. The observed opaque frequency ranges have been successfully compared with the band gaps obtained by the band calculations on the infinite periodic lattices,[3,7] for which Bloch's theorem is applicable to the relevant Maxwell equations and the computational task is much reduced. In usual analyses, the amount of the coupling between the external and the internal fields at the surface of the specimen is not taken into consideration at all.

However, the theoretical investigation on the boundary value problems, which allows for the external field, is necessary for the precise analysis of the transmission spectra. In fact, we have solved the boundary value problem for a two-dimensional (2D) triangular lattice in a previous paper[16] and shown that (1) the strength of the coupling between the incident/transmitted radiation and the internal field at the surface of the specimen substantially modifies the spectrum. Particularly, there is an uncoupled mode that cannot be excited with an external plane wave at normal incidence. (2) A considerable amount of the energy transfer to Bragg waves is expected for an incident wave whose wavelength is shorter than the lattice period parallel to the surface. (3) The transmission spectrum has quite pronounced structures due to the interference between the front and the rear surface of the specimen. [Item (1) was also discussed by Robertson *et al.* from the viewpoint of the symmetry of the wave functions for the relevant infinite lattice.[8]] Therefore, the simple analysis based on the band calculation is not sufficient and the theoretical investigation on the specimens with finite thickness is important for proper understanding of the experimental observation.

Several authors have calculated the transmission and reflection spectra of periodic dielectric structures. Ohtaka formulated the layer iteration method for vector electromagnetic waves to calculate the transmission and reflection coefficients of an array of dielectric spheres.[17] The reflectivities of monolayers of dielectric rods and spheres were calculated by Ohtaka and Numata,[18] and Inoue, Ohtaka, and Yanagawa,[19] respectively. The transmission coefficients of seven layers of a square array of dielectric rods was calculated by Pendry and MacKinnon by means of a finite-element method.[9] The last authors showed the agreement between their calculation and the experimental observation by Robertson *et al.*[8]

In the previous paper,[16] we presented a brief description of the method for calculating the transmission spectra of the 2D triangular photonic lattice that is composed of circular rods and the background dielectric with mutually different dielectric constants. We also showed some results of the numerical calculations of the transmission spectra. Our method is based on the plane-wave expansion of the electromagnetic field and is applicable to any 2D photonic lattice. It gives the transmission, the specular reflection, and the Bragg reflection coefficients. The

existence of an uncoupled mode, for which the electric field is parallel to the rod axis (E polarization) and the wave vector lies in the Γ-J direction[20] in the first Brillouin zone, was concluded from the fact that there is a spectral range where the calculated transmittance is extremely low although the state density is nonzero. Recently, the existence of this uncoupled mode was confirmed experimentally for a 2D air-rod lattice formed in a block of methylpentene polymer in the far-infrared region.[21]

In this paper, we will present the full description of the calculation and apply it to 2D triangular and square lattices. In addition to the transmission spectra, the Bragg reflection spectra will be numerically calculated and discussed in detail. In Sec. II, the boundary value problem will be formulated in a manner that is suitable to the plane-wave expansion. Both the field equations and the dielectric constant will be expressed in Fourier series. The results of the numerical calculations with an estimation of the convergence will be presented in Sec. III.

II. THEORY

A. Field equation

Our method is based on the Fourier expansion of the internal field and the dielectric structure, and is applicable to any 2D photonic lattice. We assume that the specimen is uniform along one spatial direction, which we denote by z axis, and the wave vector of the incident plane wave is perpendicular to this direction.

An example of the configuration for our calculation, where the specimen is a 2D triangular assembly of circular rods, is shown in Fig. 1 of Ref. 16. The external plane wave in region 1 is incident on the left (front) surface of the specimen located in region 2, which consists of $2N_L$ layers of circular rods with radius of R and the background dielectric. The dielectric constant of the rods and the background is denoted by ϵ_a and ϵ_b, respectively. The lattice period parallel and perpendicular to the surface is denoted by a_1 and a_2, and the distance between the surface and the first layer of the rods by d. The dielectric constant of regions 1 and 3 is ϵ_1 and ϵ_3, respectively. The total thickness L of the specimen is $L = (N_L - 0.5)a_2 + 2(R + d)$ in this example.

The electromagnetic field in region 1 is the superposition of the incident plane wave and the reflected Bragg waves, whereas that in region 3 is composed of the transmitted Bragg waves. Here we consider the specular reflection and the straight transmission as the reflected and the transmitted Bragg waves of the zeroth order. The 2D wave vector of the incident plane wave is denoted by $\mathbf{k}_i = (k_1 \sin\theta, k_1 \cos\theta) = (k_x, k_{1y})$, where θ is the angle of incidence and $k_1 = \sqrt{\epsilon_1}\omega/c$. ω is the angular frequency of the incident field and c is the light velocity in vacuum. The wave vectors of the reflected and the transmitted Bragg waves of order n, $\mathbf{k}_r^{(n)}$ and $\mathbf{k}_t^{(n)}$, are given by

$$k_{r,x}^{(n)} = k_{t,x}^{(n)} = k_x^{(n)} = k_x + G_n, \tag{1}$$

$$G_n = 2\pi n/a_1 \quad (n = 0, \pm 1, \pm 2, \ldots), \tag{2}$$

$$k_{r,y}^{(n)} = \begin{cases} -\sqrt{k_1^2 - (k_x^{(n)})^2} & \text{if } k_1 \geq |k_x^{(n)}| \\ -i\sqrt{(k_x^{(n)})^2 - k_1^2} & \text{otherwise,} \end{cases} \tag{3}$$

$$k_{t,y}^{(n)} = \begin{cases} \sqrt{k_3^2 - (k_x^{(n)})^2} & \text{if } k_3 \geq |k_x^{(n)}| \\ i\sqrt{(k_x^{(n)})^2 - k_3^2} & \text{otherwise.} \end{cases} \tag{4}$$

Here, $k_3 = \sqrt{\epsilon_3}\omega/c$. Because of the spatial periodicity along the x axis, the reflected and the transmitted Bragg waves receive a momentum along the x axis that is a multiple of $2\pi/a_1$ in Eq. (1).

The vector wave equations derived from Maxwell's equations can be reduced to two independent scalar equations when the wave vector lies in the 2D plane, or in other words, the fields are independent of the z coordinate.[10–12] These two modes are called H polarization, for which the magnetic field is parallel to the z axis, and E polarization, for which the electric field is parallel to the z axis, respectively. Because of the continuity condition for the tangential component of the magnetic or the electric field at each boundary, the fields in regions 1 and 3 are also characterized by these polarizations. The field equation and the boundary conditions for H polarization under the plane-wave expansion were given in Eqs. (17), (18), and (19) in Ref. 16. Here, we will derive them for E polarization.

The electric field in region 2 (E_{2z}) satisfies the following equation, which is derived from Maxwell's equations:[12]

$$\mathcal{L}_E[E_{2z}] = \left[\frac{1}{\epsilon(x,y)}\left(\frac{\partial^2}{\partial x^2} + \frac{\partial^2}{\partial y^2}\right) + \frac{\omega^2}{c^2}\right] E_{2z} = 0, \tag{5}$$

where $\epsilon(x,y)$ is the position-dependent dielectric constant of the specimen. The electric fields in region 1 (E_{1z}) and region 3 (E_{3z}) are given by

$$E_{1z}(x,y) = E_0 \exp(i\mathbf{k}_i \cdot \mathbf{x}) + \sum_{n=-\infty}^{\infty} R_n^{(E)} \exp(i\mathbf{k}_r^{(n)} \cdot \mathbf{x}), \tag{6}$$

$$E_{3z}(x,y) = \sum_{n=-\infty}^{\infty} T_n^{(E)} \exp\{i\mathbf{k}_t^{(n)} \cdot (\mathbf{x} - \mathbf{L})\}, \tag{7}$$

where E_0, $R_n^{(E)}$, and $T_n^{(E)}$ are the amplitude of the electric field of the incident wave, the reflected Bragg wave, and the transmitted Bragg wave, respectively. $\mathbf{x}$ stands for the 2D position vector, (x,y), and $\mathbf{L} = (0, L)$. We should note that we have to include in Eqs. (6) and (7) the localized waves with imaginary wave vectors in order to satisfy the boundary conditions at the two surfaces of the specimen. Now, we introduce a boundary value function $f_E(x,y)$:

$$f_E(x,y) = \frac{1}{L}\sum_{n=-\infty}^{\infty}\{yT_n^{(E)} + (L-y) \times(\delta_{n0}H_0 + R_n^{(E)})\}\exp(ik_x^{(n)}x), \quad (8)$$

where δ_{nm} is the Kronecker's δ. Then, f_E is equal to E_{1z} or E_{3z} on each surface of the specimen:

$$f_E(x,0) = E_{1z}(x,0) \text{ and } f_E(x,L) = E_{3z}(x,L). \quad (9)$$

Moreover, we define ψ_E as

$$\psi_E(x,y) = E_{2z}(x,y) - f_E(x,y). \quad (10)$$

Then, from Eqs. (5) and (10),

$$\mathcal{L}_E[\psi_E] = -\mathcal{L}_E[f_E], \quad (11)$$

$$\psi_E(x,0) = \psi_E(x,L) = 0. \quad (12)$$

By means of this mathematical trick, we have converted the boundary conditions for E_{2z} into the field equation of ψ_E.[22] By this procedure, we can relate the internal field in region 2 to E_0 at the first stage of the calculation, thereby we can obtain the solution of the forced oscillation and exclude the free oscillation. The choice of f_E is arbitrary as long as Eq. (9) is satisfied.

Now, we expand $\psi_E(x,y)$ and $1/\epsilon(x,y)$ in Fourier series:

$$\psi_E(x,y) = \sum_{n=-\infty}^{\infty}\sum_{m=1}^{\infty} A_{nm}^{(E)}\exp(ik_x^{(n)}x)\sin\frac{m\pi}{L}y, \quad (13)$$

$$\frac{1}{\epsilon(x,y)} = \sum_{n=-\infty}^{\infty}\sum_{m=-\infty}^{\infty}\kappa_{nm}\exp\left[i\left(G_n x + \frac{m\pi}{L}y\right)\right]. \quad (14)$$

Substituting Eqs. (8), (13), and (14) into Eq. (11) and comparing the independent Fourier components, we obtain the following equation after a simple but lengthy calculation:

$$\frac{\omega^2}{c^2}A_{nm}^{(E)} + \sum_{n'=-\infty}^{\infty}\sum_{m'=1}^{\infty}\left\{(k_x^{(n')})^2 + \left(\frac{m'\pi}{L}\right)^2\right\}(\kappa_{n-n',m+m'} - \kappa_{n-n',|m-m'|})A_{n'm'}^{(E)}$$
$$= -\frac{2\omega^2}{\pi c^2}\frac{(-1)^{m-1}T_n^{(E)} + R_n^{(E)} + \delta_{n0}E_0}{m} + \frac{2}{\pi}\sum_{n'=-\infty}^{\infty}(k_x^{(n')})^2\sum_{m'=1}^{\infty}(\kappa_{n-n',|m-m'|} - \kappa_{n-n',m+m'}) \times\frac{(-1)^{m'-1}T_{n'}^{(E)} + R_{n'}^{(E)} + \delta_{n'0}E_0}{m'}. \quad (15)$$

In deriving Eq. (15), the following two relations were used:

$$y = \frac{2L}{\pi}\sum_{m=1}^{\infty}\frac{(-1)^{m-1}}{m}\sin\frac{m\pi}{L}y, \quad (16)$$

$$1 = \frac{2}{\pi}\sum_{m=1}^{\infty}\frac{1-(-1)^m}{m}\sin\frac{m\pi}{L}y. \quad (17)$$

The remainder boundary conditions are the continuity of the x component of the magnetic field and the y component of the magnetic flux density. The latter proves to be equivalent to the continuity of the z component of the electric field and does not have to be considered. Then, the former condition at both boundaries leads to

$$\pi\sum_{m=1}^{\infty}mA_{nm}^{(E)} = (iLk_{r,y}^{(n)} + 1)R_n^{(E)} - T_n^{(E)} + \delta_{n0}E_0(iLk_{1,y} + 1), \quad (18)$$

$$\pi\sum_{m=1}^{\infty}m(-1)^m A_{nm}^{(E)} = R_n^{(E)} + (iLk_{t,y}^{(n)} - 1)T_n^{(E)} + \delta_{n0}E_0. \quad (19)$$

Equations (15), (18), and (19) determine the unknown coefficients, $A_{nm}^{(E)}$, $R_n^{(E)}$, and $T_n^{(E)}$.

B. Fourier transform of the dielectric constant

Now, the next task is to calculate the Fourier coefficients of the 2D position-dependent dielectric constant. We will show two cases as examples. They are a triangular and a square lattice of circular rods.

1. *Triangular lattice*

We will calculate the Fourier coefficients of the configuration shown in Fig. 1 of Ref. 16. In this case,

$$\frac{1}{\epsilon(x,y)} = \frac{1}{\epsilon_b} + \left(\frac{1}{\epsilon_a} - \frac{1}{\epsilon_b}\right) \times\sum_{j=1}^{4}\sum_{l=-\infty}^{\infty}\sum_{l'=0}^{N_L-1}S(\mathbf{x} - \mathbf{u}(j,l,l')), \quad (20)$$

where $\mathbf{u}(j,l,l')$ is the center of each rod,

$$\mathbf{u}(1,l,l') = (a_1 l, a_2 l' + R + d), \tag{21}$$
$$\mathbf{u}(2,l,l') = [a_1(l+1/2), a_2(l'+1/2) + R + d], \tag{22}$$
$$\mathbf{u}(3,l,l') = (a_1 l, -a_2 l' - R - d), \tag{23}$$
$$\mathbf{u}(4,l,l') = [a_1(l+1/2), -a_2(l'+1/2) - R - d], \tag{24}$$

and

$$S(\mathbf{x}) = \begin{cases} 1 & (|\mathbf{x}| \le R) \\ 0 & (|\mathbf{x}| > R). \end{cases} \tag{25}$$

Note that $1/\epsilon(x,y)$ is extended symmetrically to the region of negative y ($-L \le y \le 0$) in order to calculate the Fourier coefficients. Then,

$$\begin{aligned}\kappa_{n,m} &= \frac{1}{2a_1 L}\int_0^{a_1} dx \int_{-L}^{L} dy\, \frac{1}{\epsilon(x,y)} \exp\left[-i\left(G_n x + \frac{m\pi}{L} y\right)\right] \\ &= \frac{1}{\epsilon_b}\delta_{n0}\delta_{m0} + \frac{1}{2a_1 L}\left(\frac{1}{\epsilon_a} - \frac{1}{\epsilon_b}\right)\sum_{j=1}^{4}\sum_{l=-\infty}^{\infty}\sum_{l'=0}^{N_L-1}\int_0^{a_1} dx \int_{-L}^{L} dy\; S(\mathbf{x} - \mathbf{u}(j,l,l')) \exp(-i\mathbf{G}_{nm}\cdot\mathbf{x}) \\ &= \frac{1}{\epsilon_b}\delta_{n0}\delta_{m0} + \frac{1}{2a_1 L}\left(\frac{1}{\epsilon_a} - \frac{1}{\epsilon_b}\right)\sum_{j=1}^{4}\sum_{l'=0}^{N_L-1} \exp[-i\mathbf{G}_{nm}\cdot\mathbf{u}(j,0,l')] \int_{-\infty}^{\infty} dx \int_{-\infty}^{\infty} dy\; S(\mathbf{x}) \exp(-i\mathbf{G}_{nm}\cdot\mathbf{x}),\end{aligned} \tag{26}$$

where $\mathbf{G}_{nm} = (G_n, m\pi/L)$. Now, we calculate the Fourier transform of $S(\mathbf{x})$,

$$\begin{aligned}&\int_{-\infty}^{\infty} dx \int_{-\infty}^{\infty} dy\; S(\mathbf{x}) \exp(-i\mathbf{G}_{nm}\cdot\mathbf{x}) \\ &= \int_0^R dr \int_0^{2\pi} d\varphi\; r \exp\left[iG_{nm} r \sin\left(\varphi - \frac{\pi}{2}\right)\right] \\ &= \int_0^R dr \int_0^{2\pi} d\varphi\; r \sum_{l=-\infty}^{\infty} J_l(G_{nm} r) \exp\left[il\left(\varphi - \frac{\pi}{2}\right)\right] \\ &= 2\pi \int_0^R dr\; r J_0(G_{nm} r),\end{aligned} \tag{27}$$

where J_l is the Bessel function of the lth order and $G_{nm} = |\mathbf{G}_{nm}| = [G_n^2 + (m\pi/L)^2]^{1/2}$. We have used the following relation to derive Eq. (27):

$$\exp(iw\sin\phi) = \sum_{l=-\infty}^{\infty} J_l(w) \exp(il\phi). \tag{28}$$

Using the relation

$$\{wJ_1(w)\}' = wJ_0(w), \tag{29}$$

we obtain

$$\int_{-\infty}^{\infty} dx \int_{-\infty}^{\infty} dy S(\mathbf{x}) \exp(-i\mathbf{G}_{nm}\cdot\mathbf{x}) = \frac{2\pi R}{G_{nm}} J_1(G_{nm} R). \tag{30}$$

Next, we calculate the summation over j and l' in Eq. (26). We define S_j ($j = 1 \cdots 4$) as

$$S_j = \sum_{l'=0}^{N_L-1} \exp[-i\mathbf{G}_{nm}\cdot\mathbf{u}(j,0,l')]. \tag{31}$$

Then,

$$S_1 = \begin{cases} \exp[-im\pi(R+d)/L] \\ \quad \times \dfrac{1-\exp[-imN_L a_2\pi/L]}{1-\exp[-ima_2\pi/L]} & (m \ne 0) \\ N_L & (m = 0), \end{cases} \tag{32}$$

$$S_2 = (-1)^n \exp\left(-i\frac{ma_2\pi}{2L}\right) S_1, \tag{33}$$

$$S_3 = S_1^* \quad \text{and} \quad S_4 = S_2^*. \tag{34}$$

Finally, we obtain

$$\kappa_{0,0} = \frac{f_1}{\epsilon_a} + \frac{1-f_1}{\epsilon_b}, \tag{35}$$

$$\kappa_{2n,2m} = \begin{cases} \dfrac{2f_1}{N_L}\left(\dfrac{1}{\epsilon_a} - \dfrac{1}{\epsilon_b}\right)(-1)^m \cos\dfrac{a_2 m\pi}{2L} \dfrac{\sin(a_2 m N_L\pi/L)}{\sin(a_2 m\pi/L)} \dfrac{J_1(G_{2n,2m}R)}{G_{2n,2m}R} & (m \ne 0) \\ 2f_1\left(\dfrac{1}{\epsilon_a} - \dfrac{1}{\epsilon_b}\right)\dfrac{J_1(G_{2n}R)}{G_{2n}R} & (n \ne 0, m = 0), \end{cases} \tag{36}$$

$$\kappa_{2n-1,2m-1} = \frac{2f_1}{N_L}\left(\frac{1}{\epsilon_a} - \frac{1}{\epsilon_b}\right)(-1)^{m-1} \sin\frac{a_2(2m-1)\pi}{4L} \frac{\sin\{[a_2(2m-1)N_L\pi]/2L\}}{\sin\{[a_2(2m-1)\pi]/2L\}} \frac{J_1(G_{2n-1,2m-1}R)}{G_{2n-1,2m-1}R}, \tag{37}$$

where f_1 is the filling factor of the triangular lattice:

$$f_1 = \frac{2N_L\pi R^2}{a_1 L}. \tag{38}$$

Other $\kappa_{n,m}$'s are zero.

2. *Square lattice*

Next, we will calculate the Fourier coefficients of the configuration shown in Fig. 1. Notations in Fig. 1 are similar to those in Fig. 1 of Ref. 16 and $L = (N_L - 1)a_2 + 2(R + d)$. In this case,

$$\frac{1}{\epsilon(x,y)} = \frac{1}{\epsilon_b} + \left(\frac{1}{\epsilon_a} - \frac{1}{\epsilon_b}\right) \times \sum_{j=1}^{2} \sum_{l=-\infty}^{\infty} \sum_{l'=0}^{N_L-1} S(\mathbf{x} - \mathbf{v}(j,l,l')), \tag{39}$$

where $\mathbf{v}(j,l,l')$ is given by

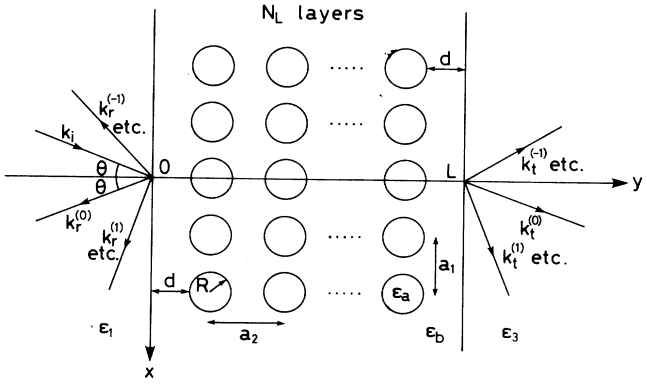

FIG. 1. A configuration for the calculation of the transmission and the Bragg reflection spectra (top view). See text for detail.

$$\mathbf{v}(1,l,l') = (a_1 l, a_2 l' + R + d), \tag{40}$$

$$\mathbf{v}(2,l,l') = (a_1 l, -a_2 l' - R - d). \tag{41}$$

A similar calculation as for the triangular lattice leads to

$$\kappa_{n,m} = \begin{cases} \dfrac{f_2}{\epsilon_a} + \dfrac{1-f_2}{\epsilon_b} & (n = 0, m = 0) \\ 2f_2\left(\dfrac{1}{\epsilon_a} - \dfrac{1}{\epsilon_b}\right)\dfrac{J_1(G_{n,m}R)}{G_{n,m}R} & (n \neq 0, m = 0) \\ \dfrac{2f_2}{N_L}\left(\dfrac{1}{\epsilon_a} - \dfrac{1}{\epsilon_b}\right)\cos\dfrac{m\pi}{2}\,\dfrac{\sin[(a_2 m N_L\pi)/2L]}{\sin[(a_2 m\pi)/2L]}\,\dfrac{J_1(G_{n,m}R)}{G_{n,m}R} & (m \neq 0), \end{cases} \tag{42}$$

where f_2 is the filling factor of the square lattice:

$$f_2 = \frac{N_L\pi R^2}{a_1 L}. \tag{43}$$

III. RESULTS AND DISCUSSION

In order to calculate the transmission and the Bragg reflection spectra numerically, we restrict the Fourier expansions up to $n = \pm N$ and $m = M$. Then, both the number of the unknown factors and the number of the independent equations are $(2N + 1)(M + 2)$. So, the problem is well defined.

Before we proceed to the results of the numerical calculation, we would like to comment on the energy conservation. In the following calculation, we assume for simplicity that the dielectric constant is real, and therefore, there is no energy dissipation. (This assumption is, of course, not substantial for the present method and we can treat complex dielectric constants as well.) Now, let us think of two flat planes that are perpendicular to the y axis, one in region 1 and the other in region 3. In addition, we assume that these two planes are far apart from region 2, and so, the amplitudes of the localized waves in Eqs. (6) and (7), which have an imaginary y component of the wave vector, are negligible at these planes. Then, the electromagnetic energy of the incident wave is carried away by the reflected and transmitted Bragg waves with real wave vectors. Comparing the inward and outward energy flow across these two planes, or in other words, summing up the y components of the Poynting vectors of all waves, we obtain the following relations: for E polarization,

$$\sum_{\{n\}} \frac{c}{4\pi}\frac{|k_{r,y}^{(n)}|}{k_1}\sqrt{\epsilon_1}|R_n^{(E)}|^2 + \sum_{\{n'\}} \frac{c}{4\pi}\frac{k_{t,y}^{(n')}}{k_3}\sqrt{\epsilon_3}|T_{n'}^{(E)}|^2 = \frac{c\cos\theta}{4\pi}\sqrt{\epsilon_1}|E_0|^2, \tag{44}$$

and for H polarization,

$$\sum_{\{n\}} \frac{c}{4\pi\sqrt{\epsilon_1}}\frac{|k_{r,y}^{(n)}|}{k_1}|R_n^{(H)}|^2 + \sum_{\{n'\}} \frac{c}{4\pi\sqrt{\epsilon_3}}\frac{k_{t,y}^{(n')}}{k_3}|T_{n'}^{(H)}|^2 = \frac{c\cos\theta}{4\pi\sqrt{\epsilon_1}}|H_0|^2, \tag{45}$$

where $\{n\}$ and $\{n'\}$ denote the summation over the Bragg waves with real wave vectors, and H_0, $R_n^{(H)}$, and $T_{n'}^{(H)}$ are

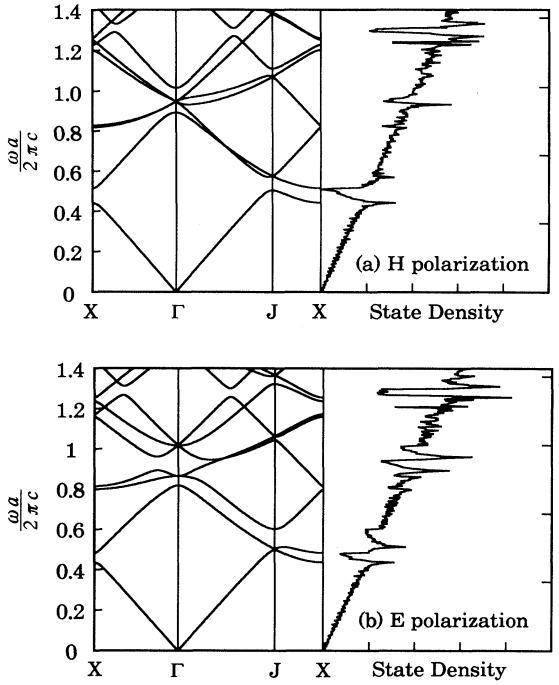

FIG. 2. The dispersion relation and the state density of the triangular lattice calculated by the plane-wave expansion method: (a) H polarization, (b) E polarization. The lattice constant a is 170 μm, the radius of the rod R is 62.5 μm, $\epsilon_a = 1.0$ (air), and $\epsilon_b = 2.1$ (methylpentene). The ordinate is the normalized frequency.

the amplitude of the magnetic field of the incident wave, the reflected Bragg wave, and the transmitted Bragg wave for H polarization, respectively. These relations can be used as an index of the accuracy of the numerical calculation. We always checked these relations while performing the following numerical calculations.

A. Triangular lattice

As we mentioned in Sec. I, the existence of an uncoupled mode, which was found theoretically in Ref. 16, was confirmed for a 2D triangular lattice of air rods formed in a block of methylpentene polymer.[21] We will examine this case in detail. The parameters designed for the experiment were as follows: the lattice constant a is 170 μm, $R = 62.5$ μm, $\epsilon_a = 1.0$ (air), $\epsilon_b = 2.1$ (methylpentene), and $\epsilon_1 = \epsilon_3 = 1.0$ (air).

First, we examine the band structure of this triangular lattice, which is shown in Fig. 2(a) for H polarization and Fig. 2(b) for E polarization. The band structure was calculated by the plane-wave expansion method according to Plihal and Maradudin.[12] Each eigenfrequency

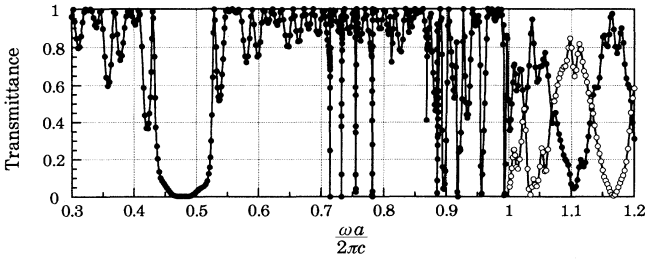

FIG. 3. The transmission (filled circles) and the Bragg reflection (open circles) spectra for H polarization along the Γ-X direction calculated for the triangular lattice composed of 14 layers ($N_L = 7$) of circular rods. The following parameters were used: $a_1 = a = 170$ μm, $a_2 = \sqrt{3}a$, $R = 62.5$ μm, $d = 900$ μm, $\epsilon_a = 1.0$ (air), $\epsilon_b = 2.1$ (methylpentene), $\epsilon_1 = \epsilon_3 = 1.0$ (air), and $\theta = 0$ (normal incidence). The abscissa is the normalized frequency.

was calculated with 271 plane waves. The convergence of the numerical calculation was checked by changing the number of basis plane waves and the error was fairly estimated as less than 1%. The state density was calculated with 28 800 wave vectors uniformly distributed in the first Brillouin zone of the 2D triangular lattice. In practice, from the symmetry of the Brillouin zone, it was sufficient to distribute 2400 wave vectors in one-twelfth of the zone. The 2D Brillouin zone of the triangular lattice possesses two relevant points beside the Γ point at the center of the zone: the J point whose wave vector is $\pi/a(4/3, 0)$ and the X point whose wave vector is $\pi/a(1, 1/\sqrt{3})$, where the elementary lattice vectors are denoted by $(a, 0)$ and $(a/2, \sqrt{3}a/2)$. We find that the first and the second bands for E polarization are degenerate at the J point and nondegenerate at the X point. On the other hand, these bands are nondegenerate at both points for H polarization. Apart from several pronounced structures, the state density increases linearly with frequency, which is typical of 2D photonic bands.

Figure 3 shows the transmission and the Bragg reflection spectra calculated for H polarization with the incident wave vector pointed to the Γ-X direction in the first Brillouin zone, or in other words, parallel to the line that connects the second nearest lattice points in the real space. Therefore, we took $a_1 = a = 170$ μm, $a_2 = \sqrt{3}a$, and $\theta = 0$ (normal incidence). In addition, we assumed that $d = 900$ μm and $N_L = 7$. The spectra in Fig. 3 were calculated with 1870 Fourier components ($N = 5$ and $M = 170$). Filled circles in Fig. 3 represent the transmittance, $|T_0^{(H)}/H_0|^2$, and open circles represent the sum of the energy flow carried away by the Bragg waves of the first order, i.e.,

$$\left[\frac{|k_{r,y}^{(1)}|}{\sqrt{\epsilon_1}k_1}|R_1^{(H)}|^2 + \frac{|k_{r,y}^{(-1)}|}{\sqrt{\epsilon_1}k_1}|R_{-1}^{(H)}|^2 + \frac{k_{t,y}^{(1)}}{\sqrt{\epsilon_3}k_3}|T_1^{(H)}|^2 + \frac{k_{t,y}^{(-1)}}{\sqrt{\epsilon_3}k_3}|T_{-1}^{(H)}|^2\right] \Big/ \left[\frac{\cos\theta}{\sqrt{\epsilon_1}}|H_0|^2\right]. \quad (46)$$

The abscissa is the normalized frequency.

In Fig. 3, we find (1) an opaque spectral range between $\omega a/2\pi c = 0.443$ and 0.518 where the transmittance is less than 0.1, which corresponds to the gap between the first and the second bands at the X point, (2) clear interference patterns caused by the front and the rear surfaces of the specimen, some of which are quite sharp and pronounced, and (3) a broad dip of the transmittance around $\omega a/2\pi c = 1.1$, which accompanies a large amount of the energy transfer to the Bragg waves. The edges of the first and the second bands at the X point are $\omega a/2\pi c = 0.443$ and 0.515, respectively. So, the correspondence between the gap and the opaque spectral range is quite good. Consequently, we can conclude that a relatively small number of the lattice layers, which is 14 ($N_L = 7$) in the present case, is enough to observe the intrinsic band structure. The interference patterns may be modified when the number of the lattice layers or the distance between the surface and the first layer is changed. We will discuss this point later in this section.

Figure 4 shows the transmission and the Bragg reflection spectra for H polarization with the incident wave vector pointed to the Γ-J direction, or, parallel to the line that connects the nearest lattice points. Therefore, we took $a_2 = a = 170$ μm, $a_1 = \sqrt{3}a$, and $\theta = 0$ (normal incidence). The other parameters are the same as for Fig. 3. In this case, the edges of the first and the second bands at the J point are $\omega a/2\pi c = 0.505$ and 0.572, respectively. We find a dip of the transmission spectrum between $\omega a/2\pi c = 0.500$ and 0.574, which again corresponds to the gap in the band structure quite well. However, the number of the lattice layer ($N_L = 7$) seems a little bit smaller than that necessary for observing the intrinsic gap in this case, since we see some structures in the dip of the transmission spectrum. We should note that the Bragg wave of the first order appears at $\omega a/2\pi c = 1/\sqrt{3}$ in Fig. 4 because the lattice period parallel to the surface of the specimen a_1 is $\sqrt{3}a$, whereas it appears at $\omega a/2\pi c = 1$ in Fig. 3 for which $a_1 = a$.

Figure 5 shows the spectra for E polarization along the Γ-X direction. The same parameters as for Fig. 3 were used. In this figure, we find two opaque spectral ranges, one between $\omega a/2\pi c = 0.436$ and 0.483, and the other between $\omega a/2\pi c = 0.895$ and 0.971. The former corresponds to the gap between the first and the second bands, whose edges are $\omega a/2\pi c = 0.437$ and 0.484, respectively. On the other hand, the latter corresponds to the gap between the fourth and the fifth bands whose edges are $\omega a/2\pi c = 0.894$ and 0.964, respectively. Again, the agreement between the band structure and the transmission spectrum is quite good. We also find a large amount of the energy transfer to the Bragg waves around $\omega a/2\pi c = 1.15$.

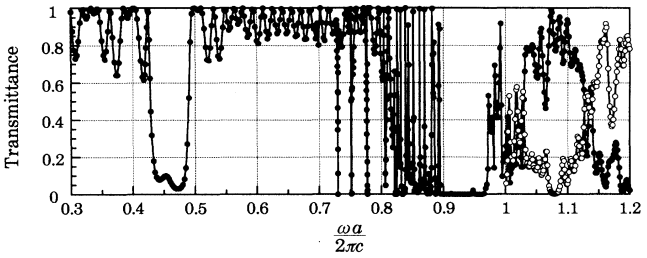

FIG. 5. The transmission (filled circles) and the Bragg reflection (open circles) spectra for E polarization at normal incidence along the Γ-X direction. The same parameters as for Fig. 3 were used.

Figure 6 shows the spectra for E polarization along the Γ-J direction. The same parameters as for Fig. 4 were used. In this case, the first and the second bands are degenerate at the J point. Therefore, no gap exists. However, we still find an opaque spectral range between $\omega a/2\pi c = 0.511$ and 0.614. As we pointed out in Ref. 16, this is due to the fact that the second band in the Γ-J direction does not couple to the external plane wave at normal incidence. Actually, the spectral range where only the second band exists is from $\omega a/2\pi c = 0.503$ to 0.604, and it agrees well with the above opaque range. This fact clearly implies that the transmission spectrum is not only governed by the state density, but also by the

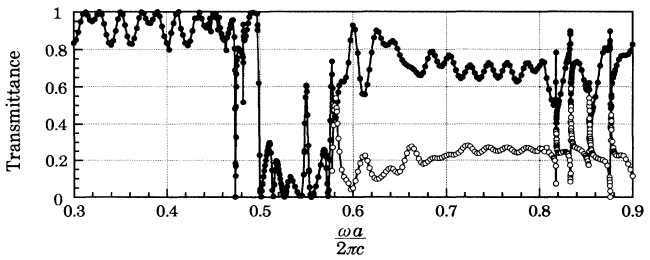

FIG. 4. The transmission (filled circles) and the Bragg reflection (open circles) spectra for H polarization along the Γ-J direction calculated for the triangular lattice composed of 14 layers ($N_L = 7$) of circular rods. $a_2 = a = 170$ μm, $a_1 = \sqrt{3}a$, and the other parameters are the same as for Fig. 3.

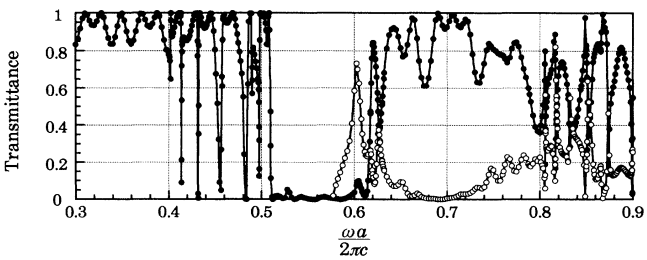

FIG. 6. The transmission (filled circles) and the Bragg reflection (open circles) spectra for E polarization at normal incidence along the Γ-J direction. The same parameters as for Fig. 4 were used.

strength of the coupling between the external and the internal fields at the surface of the specimen. Therefore, the discussion based on the state density is not sufficient for the precise analysis of the observed spectra and the theoretical investigation that allows for the coupling between the internal and the external fields is crucial.

The existence of uncoupled modes was first discussed by Robertson *et al.*[8] They compared the dispersion relation of a 2D square lattice observed by their coherent microwave transient spectroscopy technique with that by the band calculation, and found that the antisymmetric modes under the mirror reflection at the plane that is spanned by the incident wave vector and the z axis were not observed in their experiment. They argued that the incident plane wave does not excite these antisymmetric modes because the former is symmetric under the same mirror reflection, and hence, the effective coupling between them is zero. We investigated the symmetry of the wave functions in the 2D triangular lattice by the group theoretical classification based on the symmetry of the position-dependent dielectric constant, and found that the second lowest band for E polarization along the Γ-J direction is really an antisymmetric mode.[24] Therefore, our conclusion is thoroughly consistent with that of Robertson *et al.*[8]

Now, the wavy structures in each transmission spectrum, some of which are quite sharp and pronounced, are caused by the interference between the front and the rear surfaces of the specimen. The position and the depth of these structures may be modified by changing the sample parameters. As an example, we show four spectra with different N_L or d in Fig. 7. These spectra were calculated for E polarization along the Γ-J direction. The same parameters as for Figs. 4 and 6 were used except N_L and d. Fig. 7(a) is drawn for $N_L = 7$ and $d = 900$ μm, 7(b) for $N_L = 8$ and $d = 900$ μm, 7(c) for $N_L = 7$ and $d = 929$ μm, and 7(d) for $N_L = 7$ and $d = 1047$ μm. Actually, the interference pattern is modified in a rather complicated way by changing the sample parameters.

Next, the effect of oblique incidence was examined.

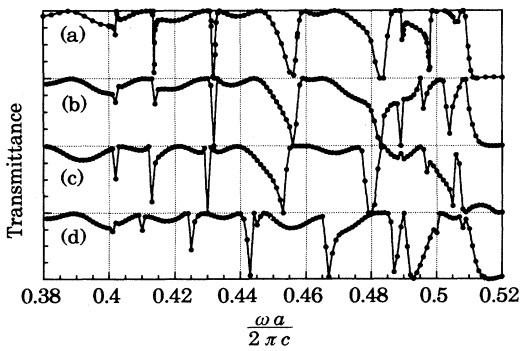

FIG. 7. The interference patterns in the transmission spectra with different values of N_L and d: (a) $N_L = 7$ and $d = 900$ μm, (b) $N_L = 8$ and $d = 900$ μm, (c) $N_L = 7$ and $d = 929$ μm, and (d) $N_L = 7$ and $d = 1047$ μm.

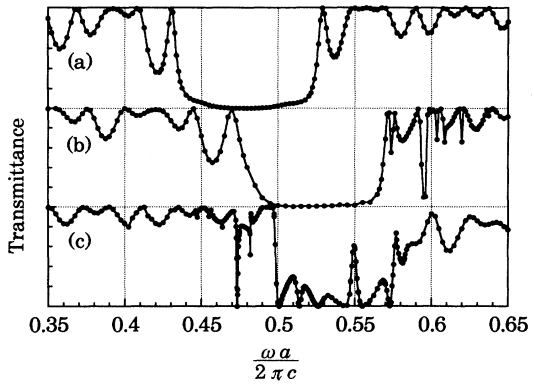

FIG. 8. The illustration of the effect of oblique incidence calculated for H polarization: (a) along the Γ-X direction at $\theta = 0°$, (b) along the Γ-J direction at $\theta = 30°$, and (c) along the Γ-J direction at $\theta = 0°$.

Three curves in Fig. 8 were calculated for H polarization. Figure 8(a) is the same as that in Fig. 3, which was obtained for the wave vector along the Γ-X direction and the angle of incidence θ is 0°. Figure 8(b) was obtained for the same configuration as 8(a) except that θ is 30°. In this case, the wave vector is regarded as to be pointed along the Γ-J direction if we neglect the effect of refraction at the surface. Figure 8(c) is the same as that in Fig. 4, which was obtained for the wave vector along the Γ-J direction and θ of 0°. We understand that the opaque spectral range is shifted to the higher frequency for oblique incidence and is nearly the same as that for the case of normal incidence along the Γ-J direction.

Finally, we would like to examine the convergence of the present calculation. The variation of $T_0^{(H)}/H_0$ with M is plotted in Fig. 9. $T_0^{(H)}/H_0$ was calculated for H polarization along the Γ-X direction at $\omega a/2\pi c = 0.6$. N

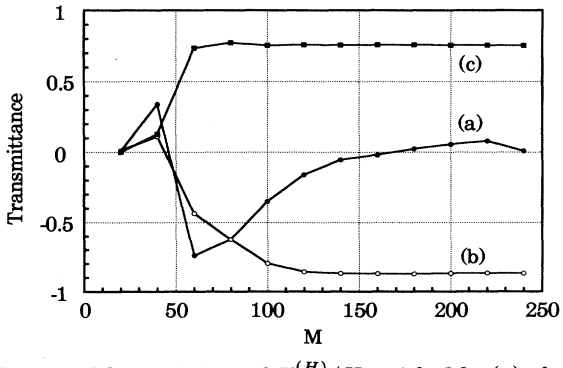

FIG. 9. The variation of $T_0^{(H)}/H_0$ with M: (a) the real part, and (b) the imaginary part of $T_0^{(H)}/H_0$, and (c) $|T_0^{(H)}/H_0|^2$. $T_0^{(H)}/H_0$ was calculated for H polarization along the Γ-X direction at $\omega a/2\pi c = 0.6$. N was fixed at 5.

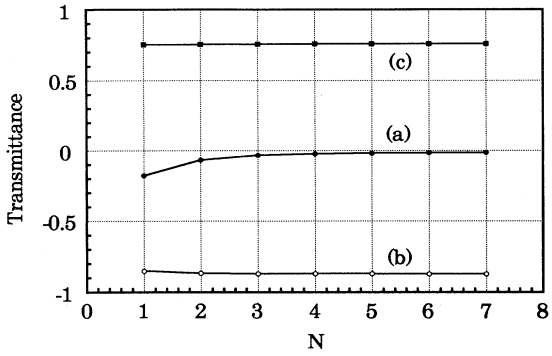

FIG. 10. The variation of $T_0^{(H)}/H_0$ with N: (a) the real part, and (b) the imaginary part of $T_0^{(H)}/H_0$, and (c) $|T_0^{(H)}/H_0|^2$. $T_0^{(H)}/H_0$ was calculated for H polarization along the Γ-X direction at $\omega a/2\pi c = 0.6$. M was fixed at 160.

was fixed at 5. Curves a, b, and c show the real part and the imaginary part of $T_0^{(H)}/H_0$ and $|T_0^{(H)}/H_0|^2$, respectively. The convergence is satisfactory for $M \geq 150$. Especially, $|T_0^{(H)}/H_0|^2$ converges very rapidly. On the other hand, Fig. 10 shows the variation of $T_0^{(H)}/H_0$ with N. M was fixed at 160. Again, the convergence is satisfactory for $N \geq 4$. The actual calculations were performed with $N = 5$ and $M = 170$ as we mentioned before. The CPU time for calculating one data point was about 10 s with a supercomputer (HITAC S-3800/380) at Hokkaido University Computing Center. When we treat a larger N_L or a larger ratio of the dielectric constants, the convergence becomes worse.

B. Square lattice

In a recent paper,[23] we reported on the 2D photonic band structure of a triangular air-rod lattice formed in a block of PbO glass, which has a full 2D band gap for H polarization in the near infrared region. Because the photonic lattices in the optical region are the possible candidates for the future investigation in the field of quantum electronics and nonlinear optics, we adopt similar parameters in the following numerical calculation as for the experiment in Ref. 23, though the lattice structure is different. Namely, we assume that the lattice constant a of the square lattice is 1.17 μm, the radius of the rod R is 0.504 μm, $\epsilon_a = 1.0$ (air), and $\epsilon_b = 2.72$ (PbO glass).

First, we calculated the dispersion relation and the state density of the square lattice by the plane-wave expansion method with 441 plane waves. The results for both H and E polarizations are shown in Fig. 11. The ordinate of the figure is the normalized frequency. The band structure is drawn for two relevant points beside the Γ point in the 2D Brillouin zone of the square lattice: the M point whose wave vector is $\pi/a(1,1)$ and the X point whose wave vector is $\pi/a(1,0)$. The state density was calculated with 9600 wave vectors uniformly distributed in the first Brillouin zone. In practice, from the symmetry of the Brillouin zone, it was sufficient to distribute 1200 wave vectors in one-eighth of the zone. As for Fig. 2, we find that the state density increases linearly with frequency.

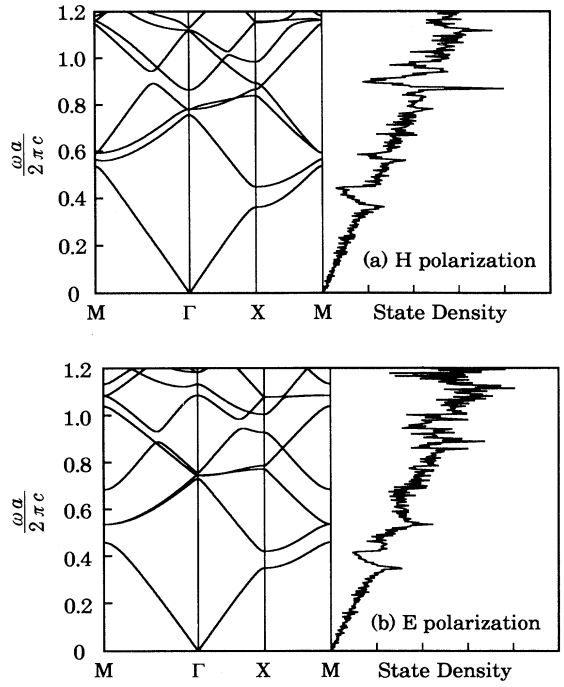

FIG. 11. The dispersion relation and the state density of the square lattice calculated by the plane-wave expansion method: (a) H polarization, (b) E polarization. The lattice constant a is 1.17 μm, the radius of the rod R is 0.504 μm, $\epsilon_a = 1.0$ (air), and $\epsilon_b = 2.72$ (PbO glass). 441 plane waves were used. The ordinate is the normalized frequency.

Now we proceed to the transmission and the Bragg reflection spectra. First, Fig. 12 shows the transmission spectrum calculated for H polarization with the incident wave vector pointed to the Γ-X direction, or in

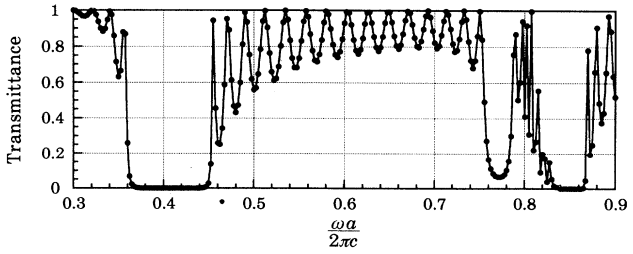

FIG. 12. The transmission spectrum for H polarization along the Γ-X direction calculated for the square lattice composed of 16 layers of circular rods. The following parameters were used in Fig. 1: $a_1 = a_2 = a = 1.17$ μm, $R = 0.504$ μm, $d = 0.081$ μm, $\epsilon_a = 1.0$ (air), $\epsilon_b = 2.72$ (PbO glass), $\epsilon_1 = \epsilon_3 = 1.0$ (air), and $\theta = 0$ (normal incidence). The abscissa is the normalized frequency.

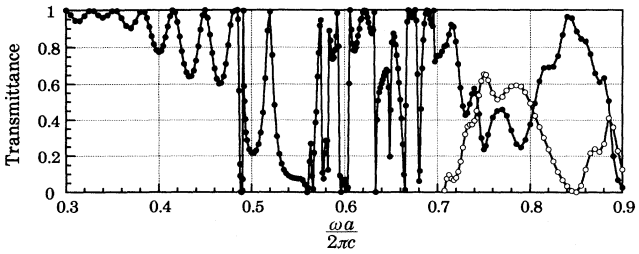

FIG. 13. The transmission (filled circles) and the Bragg reflection (open circles) spectra for H polarization along the Γ-M direction calculated for the square lattice composed of 14 layers of circular rods. The following parameters were used in Fig. 1 of Ref. 16: $a_1 = a_2 = 1.414a$, $a = 1.17$ μm, $R = 0.504$ μm, $d = 1.0$ μm, $\epsilon_a = 1.0$ (air), $\epsilon_b = 2.72$ (PbO glass), $\epsilon_1 = \epsilon_3 = 1.0$ (air), and $\theta = 0$ (normal incidence). The abscissa is the normalized frequency.

other words, parallel to the line that connects the nearest lattice points in the real space. Therefore, we took $a_1 = a_2 = a = 1.17$ μm and $\theta = 0$ (normal incidence) in Fig. 1. In addition, we assumed that $d = 0.081$ μm and $N_L = 16$. The spectrum in Fig. 12 was calculated with 2700 Fourier components ($N = 7$ and $M = 180$) and the convergence was confirmed similarly as in the previous section. As for the case of the triangular lattice, we find several opaque spectral ranges and clear interference patterns. The edges of the first and the second bands at the X point are $\omega a/2\pi c = 0.362$ and 0.448, respectively. This gap corresponds to the opaque range between $\omega a/2\pi c = 0.362$ and 0.452, where the transmittance is less than 0.1. Another opaque range is expected from $\omega a/2\pi c = 0.757$ to 0.781, which corresponds to the gap between the second and the third band in the Γ-X direction. We find a shallow spectral dip at this range. In addition, we see a broad dip around $\omega a/2\pi c = 0.85$. There are two possibilities for the origin of this dip: (1) a mere interference and (2) the null coupling between the incident plane wave and the third or the fourth band. The judgement needs a more intensive calculation on a thicker configuration with a larger N_L.

Figure 13 shows the transmission (filled circles) and the Bragg reflection (open circles) spectra for H polarization with the incident wave vector pointed to the Γ-M direction, or, parallel to the line that connects the second nearest lattice points. Therefore, we took $a_1 = a_2 = \sqrt{2}a$, $a = 1.17$ μm, $N_L = 7$, and $\theta = 0$ (normal incidence) in Fig. 1 of Ref. 16. The other parameters are the same as for Fig. 12. The open circles represent the sum of the energy flow carried away by the Bragg waves of the first order as before. In this case, the edges of the first and the second bands at the M point are $\omega a/2\pi c = 0.537$ and 0.560, respectively. We find a dip of the transmission spectrum between $\omega a/2\pi c = 0.538$ and 0.562, which again corresponds to the gap in the band structure quite well though the transmittance at the dip is not so small as that in Fig. 12. We should note that the Bragg wave of the first order appears at $\omega a/2\pi c = 1/\sqrt{2}$ in Fig. 13 because the lattice period parallel to the surface of the specimen a_1 is $\sqrt{2}a$. As for the case of the triangular lattice, we find a large amount of the energy transfer to the Bragg waves around $\omega a/2\pi c = 0.76$.

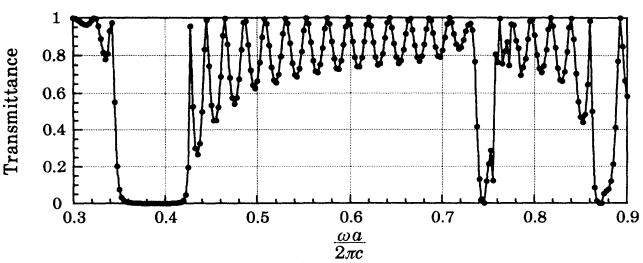

FIG. 14. The transmission spectrum for E polarization at normal incidence along the Γ-X direction. The same parameters as for Fig. 12 were used.

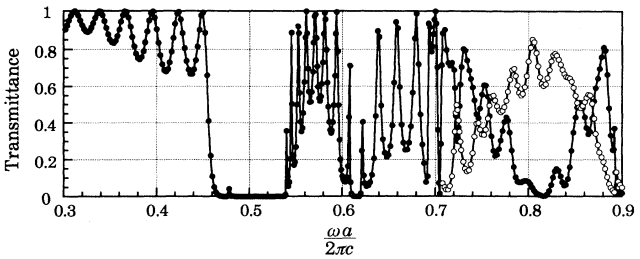

FIG. 15. The transmission (filled circles) and the Bragg reflection (open circles) spectra for E polarization at normal incidence along the Γ-M direction. The same parameters as for Fig. 13 were used.

Figure 14 shows the spectra for E polarization along the Γ-X direction. The same parameters as for Fig. 12 were used. In this figure, we find an opaque spectral range between $\omega a/2\pi c = 0.349$ and 0.423, which corresponds well to the gap between the first and the second bands whose edges are $\omega a/2\pi c = 0.348$ and 0.419, respectively. In addition, we find an opaque range around $\omega a/2\pi c = 0.74$, which corresponds to the gap between the second and the third band in the Γ-X direction.

Finally, Fig. 15 shows the spectra for E polarization along the Γ-M direction. The same parameters as for Fig. 13 were used. We find an opaque spectral range between $\omega a/2\pi c = 0.460$ and 0.539. This range agrees with the gap between $\omega a/2\pi c = 0.458$ to 0.535 quite well.

In this paper, we have calculated the transmittance and the Bragg reflectivity of 2D photonic lattices based on the Fourier expansion of the internal field and the boundary conditions at the surface of the assumed specimens. This method can be extended to three-dimensional (3D) lattices *in principle* if we take into consideration both the vector nature of the internal field and the 3D variation of the position-dependent dielectric constant. But these two items compel us to use about a 20 times larger number of basis plane waves than for the 2D lattice with the same ratio of the dielectric constants treated in this paper, and hence, the numerical calculation for the 3D lattice by this method seems impractical or it is at

least restricted to the case of a very small number of lattice layers. The development of an efficient method for 3D lattices remains a problem for future investigation.

IV. CONCLUSION

We formulated the plane-wave expansion method to calculate the transmission, the specular reflection, and the Bragg reflection coefficients of an arbitrary 2D photonic lattice, in which the boundary conditions at the surface of the specimen were rigorously taken into account. The wave vector of the incident wave was assumed to lie in the 2D plane. This assumption led to the decomposition of the vector field equation into two independent scalar equations, the solutions of which are denoted by H polarization and E polarization. Both the field equation and the boundary conditions were expressed in Fourier series, and they can be solved numerically once the Fourier coefficients of the position-dependent dielectric constant of the specimen with finite thickness is known. As examples, the coefficients were calculated for the triangular and the square lattice of circular rods, though the present method is, of course, applicable to other kinds of 2D photonic lattices.

The transmission and the Bragg reflection spectra were numerically calculated for both types of lattices mentioned above. The convergence of the calculation was confirmed by changing the number of basis plane waves. We found that the opaque frequency ranges correspond quite well to the gaps in the photonic bands, especially for the triangular lattice with 14 layers of circular rods. Therefore, we can conclude that a relatively small number of layers are enough to observe the intrinsic band structure. We also confirmed the existence of an uncoupled mode in the triangular lattice for E polarization, which cannot be excited by the external plane wave at normal incidence. In addition, we showed a large amount of energy transfer to the Bragg waves and quite sharp and pronounced interference structures for both lattices. These three optical properties of the photonic lattices, namely, the uncoupled modes, the energy transfer to the Bragg waves, and the interference structures, are not accounted for by the band calculation on the infinite periodic lattice. Hence, the theoretical investigation on the configuration with finite thickness, which fully allows for the boundary condition at the surface, is necessary for proper understanding of the observed spectra.

ACKNOWLEDGMENTS

The author is grateful to Professor K. Inoue and Professor M. Wada for stimulating discussions. This work was financially supported by the Murata Science Foundation.

[1] E. Yablonovitch, Phys. Rev. Lett. **58**, 2059 (1987).
[2] E. Yablonovitch and T. J. Gmitter, Phys. Rev. Lett. **67**, 3380 (1991).
[3] E. Yablonovitch, T. J. Gmitter, and K. M. Leung, Phys. Rev. Lett. **67**, 2295 (1991).
[4] E. Yablonovitch and T. J. Gmitter, Phys. Rev. Lett. **63**, 1950 (1989).
[5] G. Kurizki and A. Z. Genack, Phys. Rev. Lett. **61**, 2269 (1988).
[6] S. John and J. Wang, Phys. Rev. B **43**, 12 772 (1991).
[7] R. D. Meade, K. D. Brommer, A. M. Rappe, and J. D. Joannopoulos, Appl. Phys. Lett. **61**, 495 (1992).
[8] W. M. Robertson, G. Arjavalingam, R. D. Mead, K. D. Brommer, A. M. Rappe, and J. D. Joannopoulos, Phys. Rev. Lett. **68**, 2023 (1992).
[9] J. B. Pendry and A. MacKinnon, Phys. Rev. Lett. **69**, 2772 (1992).
[10] S. L. McCall, P. M. Platzman, R. Dalichaouch, D. Smith, and S. Schultz, Phys. Rev. Lett. **67**, 2017 (1991).
[11] P. R. Villeneuve and M. Piché, Phys. Rev. B **46**, 4969 (1992).
[12] M. Plihal and A. A. Maradudin, Phys. Rev. B **44**, 8565 (1991).
[13] Z. Zhang and S. Satpathy, Phys. Rev. Lett. **65**, 2650 (1990).
[14] K. M. Leung and Y. F. Liu, Phys. Rev. Lett. **65**, 2646 (1990).
[15] K. M. Ho, C. T. Chan, and C. M. Soukoulis, Phys. Rev. Lett. **65**, 3152 (1990).
[16] K. Sakoda, Phys. Rev. B **51**, 4672 (1995).
[17] K. Ohtaka, J. Phys. C **13**, 667 (1980).
[18] K. Ohtaka and H. Numata, Phys. Lett. **73A**, 411 (1979).
[19] M. Inoue, K. Ohtaka, and S. Yanagawa, Phys. Rev. B **25**, 689 (1982).
[20] After the nomenclature of Ref. 12.
[21] M. Wada (private communication).
[22] R. Courant and D. Hilbert, *Methods of Mathematical Physics* (Interscience, New York, 1953), Vol. 1, p. 277.
[23] K. Inoue, M. Wada, K. Sakoda, A. Yamanaka, M. Hayashi, and J. W. Haus, Jpn. J. Appl. Phys. **33**, L1463 (1994).
[24] K. Sakoda, Phys. Rev. B **52**, 7982 (1995).